Increasing frequency of extreme El Niño events due to greenhouse warming

Wenju Cai[1], Simon Borlace[1], Matthieu Lengaigne[2], Peter van Rensch[1], Mat Collins[3], Gabriel Vecchi[4], Axel Timmermann[5], Agus Santoso[6], Michael J. McPhaden[7], Lixin Wu[8], Matthew England[6], Eric Guilyardi[2,9], and Fei-Fei Jin[5]

1. CSIRO Marine and Atmospheric Research, Aspendale, Victoria, Australia
2. Laboratoire d'Océanographie et du Climat: Expérimentation et Approches Numériques (LOCEAN), IRD/UPMC/CNRS/MNHN, Paris, France
3. College of Engineering Mathematics and Physical Sciences, Harrison Building, Streatham Campus, University of Exeter, Exeter, UK
4. Geophysical Fluid Dynamics Laboratory/NOAA, Princeton, New Jersey, USA
5. IPRC, Department of Oceanography, SOEST, University of Hawaii, Honolulu, Hawaii , USA
6. Climate Change Research Centre and ARC Centre of Excellence for Climate System Science, University of New South Wales, Sydney, Australia
7. NOAA/Pacific Marine Environmental Laboratory, Seattle, Washington, USA
8. Ocean University of China, Qingdao, China
9. NCAS-Climate, University of Reading, Reading, UK

Wenju Cai: Wenju.Cai@csiro.au
Simon Borlace: Simon.Borlace@csiro.au
Matthieu Lengaigne: Matthieu.Lengaigne@locean-ipsl.upmc.fr
Peter van Rensch: Peter.vanRensch@csiro.au
Mat Collins: M.Collins@exeter.ac.uk
Gabriel Vecchi: gabriel.a.vecchi@noaa.gov
Axel Timmermann: axel@hawaii.edu
Agus Santoso: a.santoso@unsw.edu.au
Michael J. McPhaden: michael.j.mcphaden@noaa.gov
Lixin Wu: lxwu@ouc.edu.cn
Matthew England: m.england@unsw.edu.au
Eric Guilyardi: Eric.Guilyardi@locean-ipsl.upmc.fr
Fei-Fei Jin: jff@hawaii.edu

El Niño events, characterised by an anomalous warming in the eastern equatorial Pacific Ocean, are a prominent feature of climate variability with global climatic impacts. The 1997/98 episode, often referred to as "the climate event of the 20th century[1-3]", and the 1982/83 extreme El Niño[4], were characterized by a pronounced eastward extension of the west Pacific warm pool and development of an atmospheric convective zone, and hence a huge rainfall increase in the usually cold and dry equatorial eastern Pacific. Such a massive reorganization of atmospheric convection, which we define as an "extreme El Niño" in this study, severely disrupted global weather patterns, affecting ecosystems[5, 6], agriculture[7], tropical cyclones, drought, bushfires, floods and other extreme weather events worldwide[4,8-11]. Potential future changes in the frequency of such extreme El Niño events could hence have profound socio-economical consequences. Here we present climate modelling evidence for a doubling in the occurrence of extreme El Niño events in the future in response to greenhouse warming. We focus on convection and rainfall in the eastern equatorial Pacific, and estimate the change by aggregating results from climate models in the Coupled Model Intercomparison Project phases 3 and 5 (CMIP3[12] and CMIP5[13]) multi-model databases, and perturbed physics ensembles (PPEs)[14], selected by their ability to reproduce processes that give rise to extreme El Nino events. The increased frequency arises from a projected faster warming along the equatorial Pacific compared to off-equatorial regions, and in the eastern equatorial Pacific more so than in the west[15,16], facilitating more occurrences of atmospheric convection in the eastern equatorial Pacific for a given anomalous warming.

During the 1982/83 and 1997/98 extreme El Niño events, the western Pacific warm pool (water with sea surface temperatures (SSTs) higher than 28°C) and associated convective rainfall extended far into the eastern equatorial Pacific[3,4]. This severely disrupted global weather patterns and led to major natural disasters. Catastrophic floods occurred in the eastern equatorial region of Ecuador and northern Peru, with the annual rainfall total up to an order of magnitude larger than during normal conditions[4, 17], whereas neighbouring regions to the south and north experienced severe droughts (Supplementary Fig. 1). The anomalous conditions caused severe

rainfall deficits in the western Pacific and the Maritime Continent, devastating hurricanes in the central tropical Pacific region (where such phenomena are extremely rare[4, 8, 10, 11]), and the disappearance of marine life and decimation of the native bird population on Christmas Island[17, 18]. The high SSTs led to severe bleaching of corals in the Pacific and beyond[5, 6], including the 1998 mass mortality of corals on lagoonal reefs in Belize – the first time a coral population in the Caribbean collapsed completely from bleaching[6]. The impact extended to every continent, and the 1997/98 event alone caused $35–45 US billion in damage and took an estimated 23,000 human lives worldwide[19].

In view of the devastating impacts, it is essential to determine whether greenhouse warming will alter the frequency of extreme El Niño events. Although many studies have examined the effects of a projected warming on the Pacific mean state, El Niño diversity and El Niño in general[20-23], the issue of how extreme El Niño events will change has not yet been investigated. Here we show how greenhouse warming can lead to a significant increase in the frequency of such extreme events.

We characterise the observed extreme El Niño events by their differences from moderate events using available datasets[24, 25], focusing on austral summer (December-January-February, DJF), the season in which El Niño events peak. During moderate events, the eastern boundary of the warm pool (indicated by the 28°C isotherm, purple, Fig. 1a) and the atmospheric convective zone move eastwards to just east of the Dateline. The Intertropical Convergence Zone (ITCZ) is located just north of the equator[26, 27], and the rainfall anomaly over the eastern equatorial Pacific is small (Fig. 1a).

During extreme El Niño events, the warm pool extends into the eastern equatorial Pacific[3,4], and eventually covers the entire equatorial Pacific, dramatically weakening the equatorial east-west SST gradient and the meridional SST gradient between the eastern off-equatorial region (8°N, the climatological position of the ITCZ) and the equatorial Pacific (Fig. 1d, Supplementary Fig. 2a and c). Consequently convection, which follows the warmest SSTs, extends eastward and the ITCZ shifts equatorward[26, 27], leading to the development of an atmospheric convective zone and extraordinary rainfall (greater than 5 mm per day, indicated by the green curve, Fig.

1b) in the normally dry eastern equatorial Pacific. The easterly winds in the central Pacific are replaced by westerlies, which suppress the eastern equatorial upwelling[3, 4], reinforcing the exceptionally high SSTs in this region, severely weakening or reversing zonal and meridional SST gradients, and inducing the equatorward displacement of the ITCZ.

A diminishing meridional gradient in the eastern equatorial Pacific is an excellent indicator for the eastward extension and the equatorward shift of the atmospheric convective zones, as it also reflects changes in zonal SST gradients (Supplementary Fig. 3). In association, Niño3 rainfall increases nonlinearly with Niño3 SST (Fig. 1c), and the meridional SST gradient (Fig. 1d). This striking nonlinearity highlights a distinct feature of extreme El Niño. Niño3 area-averaged rainfall, or its equivalent, the outgoing longwave radiation[27, 28], is a good indicator of extreme El Niño because it is the anomalous convection and rainfall that influence global weather impacts. In particular, rainfall is an excellent measure for condensational heating of the atmosphere, thus providing an effective metric for large-scale atmospheric circulation changes. The rainfall nonlinearity can be measured by the skewness of its probability distribution, and is 2.75 in observations over the period since 1979. We define an extreme El Niño event as occurring when a massive reorganisation of atmospheric convection takes place such that Niño3 rainfall exceeds 5 mm per day, similar to a previous definition using a Niño3 rainfall anomaly[27]. This definition distinctively identifies the 1982/83 and 1997/98 events as extreme El Niños.

Not all coupled general circulation models (CGCMs) from the CMIP3[12] and CMIP5[13] databases are able to simulate this nonlinearity. The CMIP3 and CMIP5 CGCMs are forced with historical anthropogenic and natural forcings, and future greenhouse gas emission scenarios of Special Report on Emission Scenarios A2 (SRESA2) and Representative Concentration Pathway (RCP) 8.5, respectively, each covering a 200-year period. We include only CGCMs whose Niño3 rainfall skewness exceeds 1 over the 200-year period. Nine CMIP3 and eleven CMIP5 CGCMs, which produce this level of nonlinearity *and* Niño3 rainfall greater than 5 mm per day, are selected (Supplementary Figs 4–7 and Tables 1–2). Our definition of extreme El Niño avoids a common CGCM bias of overly low SSTs in the eastern equatorial Pacific[20, 21], which may make an SST definition unreliable, because the same SST anomaly can

generate vastly different convective responses in different models. From these 20 CGCMs, we compare the frequency of extreme El Niño events in the first (1891–1990) and second (1991–2090) 100-year periods based on raw rainfall data, referred to as the *Control* and *Climate Change* periods, respectively, to investigate the influence of greenhouse warming.

Evolution of modelled moderate and extreme El Niño events under *Control* conditions reproduces the observed contrasts (Fig. 2). These include a cross-basin eastward extension of the warm pool, an eastward extension of the west Pacific convective zone and an equatorward shift of the ITCZ (Supplementary Fig. 2b and d) generating a large rainfall increase in the eastern equatorial Pacific during extreme El Niño (Fig. 2b, Supplementary Fig. 8). These features are absent during moderate events (Fig. 2a). The extreme events are caused by a partial collapse or complete reversal of the climatological meridional SST gradient in the eastern equatorial Pacific (Fig. 2c). In aggregation, the frequency doubles from about one event every 20 years (101 events in 2,000 years) in the *Control,* to one every 10 years (212 events in 2,000 years) in the *Climate Change* period (Fig. 2c and d). This is statistically significant according to a bootstrap test[29] (see Methods), underscored by a strong consensus among CGCMs, with 17 out of 20 models simulating an increase in extreme El Niño events (Supplementary Tables 1 and 2). Sensitivity tests to varying definitions of extreme El Niño (e.g. in conjunction with a diminishing meridional SST gradient, or Niño3 rainfall relative to that in the western Pacific) support the robustness of this result (Supplementary Tables 3 and 4). There is little change in the ensemble-averaged intensity (Supplementary Figs 9 and 10).

We assess the potential impact of the well-known but still unresolved cold SST bias on our result using the HadCM3 CGCM, in which biases are corrected through a fixed flux adjustment[14] in a set of PPE experiments that are able to produce extreme El Niño events. There is a four-fold increase in the frequency of extreme El Niño events; from one event in 60 years in the *Control* to one event in 15 years in the *Climate Change* period (Supplementary Fig. 11 and Table 5). Thus the conclusions drawn from CMIP3 and CMIP5 CGCMs are not influenced by the SST biases.

Development of atmospheric convection over the eastern equatorial Pacific defines an extreme El Niño event and its global impact. Such development is induced by a diminishing or reversing meridional SST gradient, which also reflects the associated reduction in zonal SST gradient (Supplementary Fig. 12). An increase in extreme El Niño events may hence arise from more frequent occurrences of diminishing or reversing meridional SST gradients. Greenhouse warming induces a faster warming rate along the equator than in the off-equatorial Pacific, and also a more rapid warming in the eastern equatorial Pacific than in the west (Supplementary Fig. 13)[15,16], even in simulations without a dynamical ocean[30]. The warming pattern thus encompasses a small decrease in the climatological meridional gradient.

These slight climatological changes in SST gradient translate into a large increase in the occurrences of a diminished or reversed meridional SST gradient (Fig. 3a). In association, there are increased occurrences of extreme El Niño events (Fig. 3b), as the slight change in the climatological SST gradient facilitates more frequent collapse or reversal of the climatological zonal and meridional SST gradient. This results in easier development of convective zones in the eastern equatorial Pacific for a given SST anomaly, even though the amplitude of SST anomalies is little changed.

The weakening background SST gradient means that the increased occurrences of extreme El Niño do not simply result from an increasing climatological rainfall, but instead from enhanced probability of the establishment of eastern equatorial Pacific deep convection. This is further illustrated in the histogram of quadratically detrended Niño3 rainfall anomalies for all El Niño events, defined as when the detrended Niño3 SST anomaly is greater than a 0.5-standard deviation value in the *Control* period (Fig. 3c). There is a 66% increase in the occurrences of rainfall anomalies greater than 3 mm per day with a strong inter-model consensus (Supplementary Table 6 and Fig. 14). In contrast, there is not as strong a line of evidence for a robust change or an inter-model consensus following the commonly-used definition based on similarly detrended Niño3 SST (Fig. 3d, Supplementary Table 7). Because of increased occurrences of atmospheric convection in the eastern equatorial Pacific, the sensitivity of rainfall to SST anomalies increases by 25% (Supplementary Fig. 15), despite the lack of a substantial change in the distribution of SST anomalies.

In summary, increased future occurrences of extreme El Niño events, as characterized by massive equatorial rainfall anomalies and the associated shift of atmospheric convection to the eastern equatorial Pacific, are facilitated by projected changes of SST gradients in the background state. Our results are in stark contrast with previous findings of no consensus in El Niño change; our robust results arise from the use of process-based metrics, such as SST gradients and the impacts on reorganization of atmospheric convection, that isolate the mechanism of extreme El Niño events. With a projected large increase in extreme El Niño events, we should expect more frequent devastating weather events, which will have dramatic implications for 21st century climate.

METHODS SUMMARY

The extreme El Niño events were diagnosed in observations and in CMIP3 and CMIP5 CGCMs based on their distinctive features, including a large eastward extension of the west Pacific atmospheric convection zone and a shift of the ITCZ to the equator, leading to an enormous rainfall increase in the eastern equatorial Pacific. For observations, we focus on historical events in the satellite era (1979–present) using rainfall data[25]: Global Precipitation Climatology Project monthly precipitation analysis, as obtained from http://www.esrl.noaa.gov/psd/data/gridded/data.gpcp.html; and SSTs from a global reanalysis[24]. We average DJF rainfall over the Niño3 region (150°W-90°W, 5°S-5°N) and calculate the meridional SST gradient in the eastern equatorial Pacific (150°W-90°W) as the difference between the average over the off-equatorial (5°N–10°N) and that equatorial box (2.5°S–2.5°N). These quantities are used as atmospheric and oceanic indices to characterise extreme El Niño events. Rainfall increases nonlinearly with Niño3 SST, or with the meridional gradient. The nonlinearity is measured by the skewness of Niño3 precipitation which is greater than 2 in observations. An extreme El Niño event is defined as one for which DJF Niño3 rainfall is greater than 5 mm per day. Both this and rainfall skewness greater than 1 are used as criteria for model selection from a total of 17 CMIP3 and 21 CMIP5 CGCMs. One experiment (the first available simulation) from each model is used, covering the period 1891–2090 using historical anthropogenic and natural forcings to 2000 for CMIP3 and 2005 for CMIP5, and then a future climate emission scenario under the SRESA2 scenario for CMIP3[12] and the RCP8.5 scenario for CMIP5[13]. In

addition, 33 SST-bias corrected PPE experiments, conducted with the HadCM3 CGCM forced with historical radiative perturbations and a 1% per year CO_2 increase[14] for the future climate change runs, each covering a 200-year period, are used.

References

1. Changnon, S. A., El Niño, 1997–1998: The Climate Event of the Century. *Oxford University Press Inc.* 232.pp (2000).
2. Kerr, R. Big El Niños Ride the Back of Slower Climate Change. *Science* **283,** 1108–1109 (1999).
3. McPhaden, M. J. El Niño: The child prodigy of 1997–98. *Nature* **398**, 559–562. doi:10.1038/19193 (1999).
4. Philander, S. G. H., Anomalous El Niño of 1982–83. *Nature* **305**, 16 (1983).
5. Glynn, P. W., & de Weerdt, W. H. Elimination of two reef-building hydrocorals following the 1982–83 El Niño. *Science* **253**, 69–71 (1991).
6. Aronson, R. B., *et al.* Coral bleach-out in Belize, *Nature* **405,** 36 (2000).
7. Wilhite, D. A., Wood, D. A. & Meyer, S. J. Climate-related impacts in the United States during the 1982–83 El Niño. Climate Crisis, M. Glantz, R. Katz, and M. Krenz, Eds., UNEP, 75–78 (1987).
8. Vos, R., Velasco, M., & Edgar de Labastida, R. Economic and social effects of El Niño in Ecuador, 1997–1998. Inter-American Development Bank.Sustainable Development Dept. Technical papers series POV-107, 38pp (1999).
9. Changnon, S. A., Impacts of 1997—98 El Niño generated weather in the United States. *Bull. Amer. Meteor. Soc.* **80,** 1819–1827 (1999).
10. Vincent, E. M. *et al.* Interannual variability of the South Pacific Convergence Zone and implications for tropical cyclone genesis. *Clim. Dyn.* **36,** 1881–1896 (2011).
11. Cai, W. *et al.* More extreme swings of the South Pacific convergence zone due to greenhouse warming. *Nature* **488**, 365–369 (2012).
12. Meehl, G. et al. TheWCRP CMIP3multimodel dataset: a new era in climate change research. *Bull. Am. Meteorol. Soc.* **88**, 1383–1394 (2007).
13. Taylor, K. E., Stouffer, R. J. & Meehl, G. A. An overview of CMIP5 and the experimental design. *Bull. Amer. Met. Soc*. **93**, 485–498, doi: 10.1175/BAMS-D-11-00094.1 (2012).

14. Collins, M. *et al.* A comparison of perturbed physics and multi-model ensembles: Model errors, feedbacks and forcings. *Clim. Dyn.* **36,** 1737–1766. (2011).
15. Xie, S. P. *et al.* Global warming pattern formation: sea surface temperature and rainfall. *J. Clim.* **23,** 966–986 (2010).
16. Tokinaga, H., Xie, S.-P., Deser, C., Kosaka, Y. & Okumura, Y. M. Slowdown of the Walker circulation driven by tropical Indo-Pacific warming, *Nature* **491**, 439–443 (2012).
17. Valle C. A. *et al.* The Impact of the 1982–1983 E1 Niño-Southern Oscillation on Seabirds in the Galapagos Islands, Ecuador. *J. Geophys. Res*. **92,** 14,437–14,444, (1987).
18. Merlen, G., The 1982–1983 El Niño: Some of its consequences for Galapagos wildlife, *Oryx* **18,** 210–214 (1984).
19. Sponberg, K. Navigating the numbers of climatological impact. Compendium of Climatological Impacts, University Corporation for Atmospheric Research, Vol. 1, National Oceanic and Atmospheric Administration, Office of Global Programs, 13 pp. [Available online at http://www.cip.noaa. gov/docs/navimpact.pdf.] (1999).
20. Guilyardi, E. et al. Understanding El Niño in ocean–atmosphere general circulation models: progress and challenges. *Bull. Am. Meteorol. Soc.* **90**, 325–340 (2009).
21. Collins, M. et al. The impact of global warming on the tropical Pacific Ocean and El Niño. *Nature Geosci.* **3**, 391–397 (2010).
22. Yeh, S.-W. *et al.* El Niño in a changing climate. *Nature* **461,** 511–514 (2009).
23. Vecchi, G. A. *et al.* Weakening of tropical Pacific atmospheric circulation due to anthropogenic forcing. *Nature* **441,** 73–76 (2006).
24. Rayner, N. A. *et al*. Global analyses of sea surface temperature, sea ice, and night marine air temperature since the late nineteenth century. *J. Geophys. Res.* **108,** 4407, (2003).
25. Adler, R. F. *et al.* The version 2 Global Precipitation Climatology Project (GPCP) monthly precipitation analysis (1979–present). *J. Hydrometeor.* **4,** 1147–1167 (2003).
26. Vecchi, G. A., & Harrison, D. E. The termination of the 1997–98 El Niño. Part I: mechanisms of oceanic change. *J. Clim.* **19,** 2633–2646. doi:10.1175/JCLI3776.1 (2006).

27. Lengaigne, M., & Vecchi, G. A. Contrasting the termination of moderate and extreme El Niño events in coupled general circulation models. *Clim. Dyn.* DOI 10.1007/s00382-009-0562-3 (2009).
28. Chiodi, A. M., & Harrison, D. E. Characterizing warm-ENSO variability in the equatorial Pacific: An OLR perspective. *J. Clim.* **23**, 2428–2439 (2010).
29. Austin, P. C. Bootstrap methods for developing predictive models. *Am. Stat.* **58**, 131–137 (2004).
30. Vecchi, G.A., & Soden, B.J. Global Warming and the Weakening of the Tropical Circulation. *J. Clim*. **20,** 4316–4340 (2007).

Acknowledgements

This work is supported by the Australian Climate Change Science Program, the CSIRO Office of Chief Executive Science Leader award, and the Pacific-Australia Climate Change Science and Adaptation Planning Program.

Author Contributions

W.C. conceived the study in discussion with M.L. and G.V., and wrote the initial draft of the paper. S.B. and P. v. R. performed the analysis. M.C. conducted the perturbed physics ensemble climate change experiments with the HadCM3 model. All authors contributed to interpreting results, discussion of the associated dynamics, and improvement of this paper.

Author Information Reprints and permissions information are available at: www.nature.com/reprints. The authors declare no competing financial interests. Correspondence and requests for materials should be addressed to Wenju Cai (wenju.cai@csiro.au).

METHODS

Selection of models. Although the majority of CGCMs generate El Niño-like variability, only a subgroup of CGCMs simulate the observed nonlinear ocean-atmosphere coupling, as reflected in the skewness of the DJF rainfall over the eastern equatorial Pacific. The level of nonlinearity varies vastly among CGCMs. We use DJF Niño3 rainfall skewness greater than 1, and DJF Niño3 rainfall greater than 5 mm per day as criteria for selecting CGCMs. Out of the 38 CGCMs, only 9 CMIP3

and 11 CMIP5 CGCMs capture rainfall nonlinearity over the Niño3 area and are able to generate extreme El Niño events with Niño3 rainfall greater than 5 mm per day (Supplementary Tables 1 and 2). The selected CGCMs yield a mean skewness close to the observed (Supplementary Tables 1 and 2). Out of 33 PPE experiments, 25 simulate the observed nonlinearity. Outputs are used from experiments run from 1891–2090, under historical anthropogenic and natural forcings and then under projected climate scenarios. We derive changes in the occurrence of extreme El Niño events by comparing the frequency of the first 100 years (*Control* period) to that of the second 100 years (*Climate Change* period). We also test the sensitivity of our results to varying definitions (Supplementary Tables 3 and 4).

Extreme El Niño and zonal South Pacific Convergence Zone (SPCZ) events. Our result of a greenhouse-induced increase in extreme El Niño events is consistent with greenhouse-induced increases in zonal SPCZ events[11], in which the SPCZ swings toward the equator by up to 1,000 km, because such swings can occur concurrently with an extreme El Niño. The extreme swing causes severe droughts and bushfires in some regions and floods in others, along with severe food shortages (due to weather impacts on agriculture), unprecedented coral mortality, and a massive redistribution of tropical cyclone genesis[10, 11]. However, such swings can also occur without an extreme El Niño, as in the 1991/92 event, and rely on a diminishing meridional gradient in the western rather than the eastern equatorial Pacific. As such, the CGCMs identified for the two studies are not the same, although the majority of selected CGCMs overlap (Supplementary Tables 1 and 2).

Total rainfall change. The total rainfall change in the eastern equatorial Pacific under greenhouse warming ($\Delta Rain_{total}$) may be regarded as containing a contribution by a change in the annual cycle ($\Delta Rain_{annual\text{-}cycle}$), a long-term trend ($\Delta Rain_{long\text{-}term}$), and a change in the response of rainfall to changing El Niño-Southern Oscillation (ENSO) ($\Delta Rain_{ENSO}$). For a given season, the $\Delta Rain_{annual\text{-}cycle}$ and $\Delta Rain_{long\text{-}term}$ terms can be combined to a total long-term trend, $\Delta \mathrm{Rain}_{total\text{-}long\text{-}term}$, such that

$$\Delta Rain_{total} = \Delta Rain_{total\text{-}long\text{-}term} + \Delta Rain_{ENSO.}$$

Because ENSO is seasonally phase-locked, peaking in austral summer, if there is a trend due to the response to ENSO, the total rainfall trend will include the contribution from $\Delta Rain_{ENSO}$, which would be at least partially removed by the

detrending process. To understand how the distribution of rainfall anomalies will change, rainfall is quadratically detrended. The detrending process might partially remove the rainfall increase due to the increased frequency of extreme El Niño events.

Statistical significance test. We use a bootstrap method[29] to examine whether the change in frequency of the extreme El Niño events is statistically significant. The 2,000 DJF samples from the 20 selected CMIP3 and CMIP5 CGCMs in the *Control* period are re-sampled randomly to construct another 10,000 realisations of 2,000-year records. During the random re-sampling process, overlapping is allowed, so that any one extreme El Niño event can be selected again. The standard deviation of the extreme El Niño frequency in the inter-realisation is 9.8 events per 2,000 years, far smaller than the difference between the *Control* and the *Climate Change* periods at 111 events per 2,000 years (Fig. 2c and d), indicating statistical significance of the difference between the *Control* and the *Climate Change* periods. The maximum frequency is 139, far smaller than that in the *Climate Change* period, further highlighting the strong statistical significance of the difference between the two periods. Increasing the realisations to 15,000 yields an essentially identical result. This process is repeated for the PPE experiments to generate 10,000 realisations of 2,500 samples (for 25 PPE experiments), from their respective *Control* period, which also suggests a similarly strong statistical significance to that described above.

Figure Captions

Figure 1 | Evolution and nonlinear characteristics of observed extreme El Niño events. a and **b,** Time-longitude diagram for composite moderate and extreme El Niño events, respectively, of equatorial SST anomalies (°C, colour) and rainfall anomalies (contour, at intervals of 3 mm per day), **28°C isotherm** (**purple curve**) and **5 mm per day** isopleth (**green curve**). **c** and **d,** Relationship of eastern equatorial Pacific (Niño3 area: 5°S–5°N, 150°W–90°W) DJF total rainfall (mm per day) with DJF Niño3 SST and meridional SST gradients (°C) in the Niño3 longitude range. The meridional SST gradient is defined as the average SST over the off-equatorial region (5°N–10°N, 150°W–90°W) minus the average over the equatorial region (2.5°S–2.5°N, 150°W–90°W). **Red**, **green**, and **blue** dots indicate **extreme El Niño** (defined as events for which austral summer rainfall is greater than 5 mm per day), **moderate El Niño** (defined as events with SST anomalies greater than 0.5 standard deviation of that over the period since 1979 that are not extreme El Niño events), and **La Niña and neutral** events, respectively. During **extreme El Niño**, the meridional SST gradient diminishes, or reverses, shifting the ITCZ to the eastern equatorial Pacific.

Figure 2 | Evolution and nonlinear characteristics of model extreme El Niño events, and changes in occurrences under greenhouse warming. a and **b,** Time-longitude diagram for composite moderate and extreme El Niño events, respectively, of equatorial SST anomalies (°C, colour) and rainfall anomalies (contour, at intervals of 3 mm per day), 28°C isotherm (**purple curve**) and 5 mm per day isopleth (**green curve**) for the *Control* period, illustrating simulation of the observed evolution. **c** and **d,** Relationship between eastern equatorial Pacific (Niño3 area: 5°S-5°N, 150°W-90°W) austral summer total rainfall and austral summer meridional SST gradient for the *Control* and *Climate Change* periods, respectively. **Red**, **green**, and **blue** dots indicate **extreme El Niño** (defined as events for which austral summer rainfall is greater than 5 mm per day), **moderate El Niño** (defined as events with SST anomalies greater than 0.5 standard deviation of the *Control* period that are not extreme El Niño events), and **La Niña and neutral** events, respectively. The number of **moderate El Niño** and **extreme El Niño** events in each period is displayed.

Figure 3 | Multi-model statistics associated with the increase in the frequency of extreme El Niño events. a and **b,** Multi-model histograms of the meridional SST gradient (°C) in the eastern equatorial Pacific for all samples, and for extreme El Niño only**.** The meridional SST gradient is defined as the average SST over the east off-equatorial region (5°N–10°N, 150°E–90°W) minus the average over the eastern equatorial region (2.5°S–2.5°N, 155°E–120°W). All 2,000 samples in each period are distributed into 0.5°C bins, for the ***Control*** (**blue**) and ***Climate Change*** (**red**) periods. The multi-model climatological values for the ***Control*** (**blue** dashed line) and the ***Climate Change*** (**red** dashed line) periods are indicated. **c**, Multi-model histogram of quadratically detrended rainfall anomalies for El Niño, showing increased occurrences from ***Control*** to the ***Climate Change*** period for given positive anomalies greater than 2 mm per day. **d,** Multi-model histogram of quadratically detrended SST anomalies normalised by the standard deviation of quadratically detrended Niño3 SST anomalies of the ***Control*** period. Possible changes in El Niño are commonly examined using this approach[20, 21], which yields little change in the distribution from the ***Control*** to the ***Climate Change*** period, unlike the analysis in panel **c**.

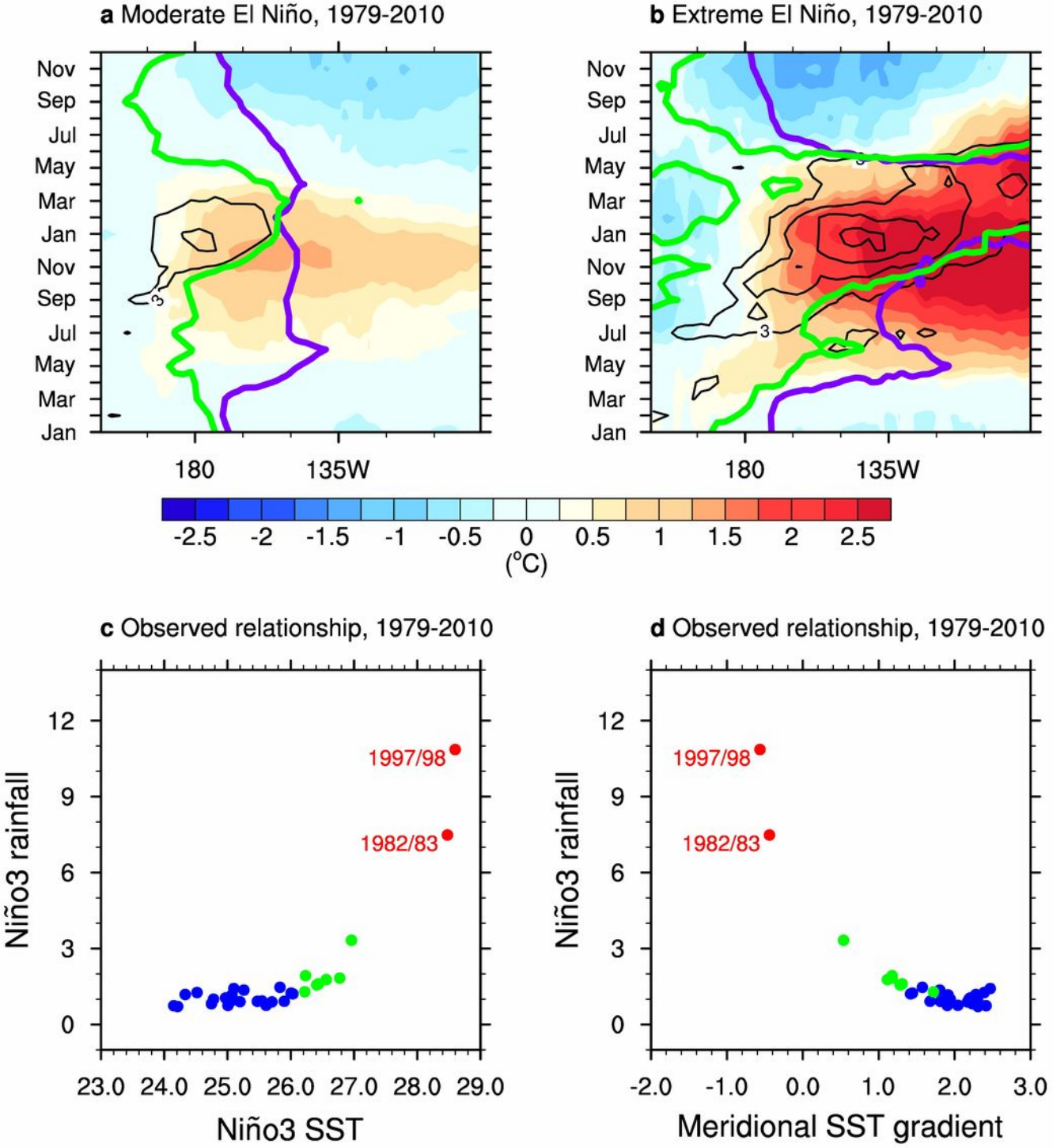
a Moderate El Niño, 1979-2010
b Extreme El Niño, 1979-2010
Nov
Sep
Jul
May
Mar
Jan
180
135W
3
-2.5 -2 -1.5 -1 -0.5 0 0.5 1 1.5 2 2.5
(°C)
c Observed relationship, 1979-2010
d Observed relationship, 1979-2010
Niño3 rainfall
Niño3 SST
Meridional SST gradient
1997/98
1982/83
0 3 6 9 12
23.0 24.0 25.0 26.0 27.0 28.0 29.0
-2.0 -1.0 0.0 1.0 2.0 3.0

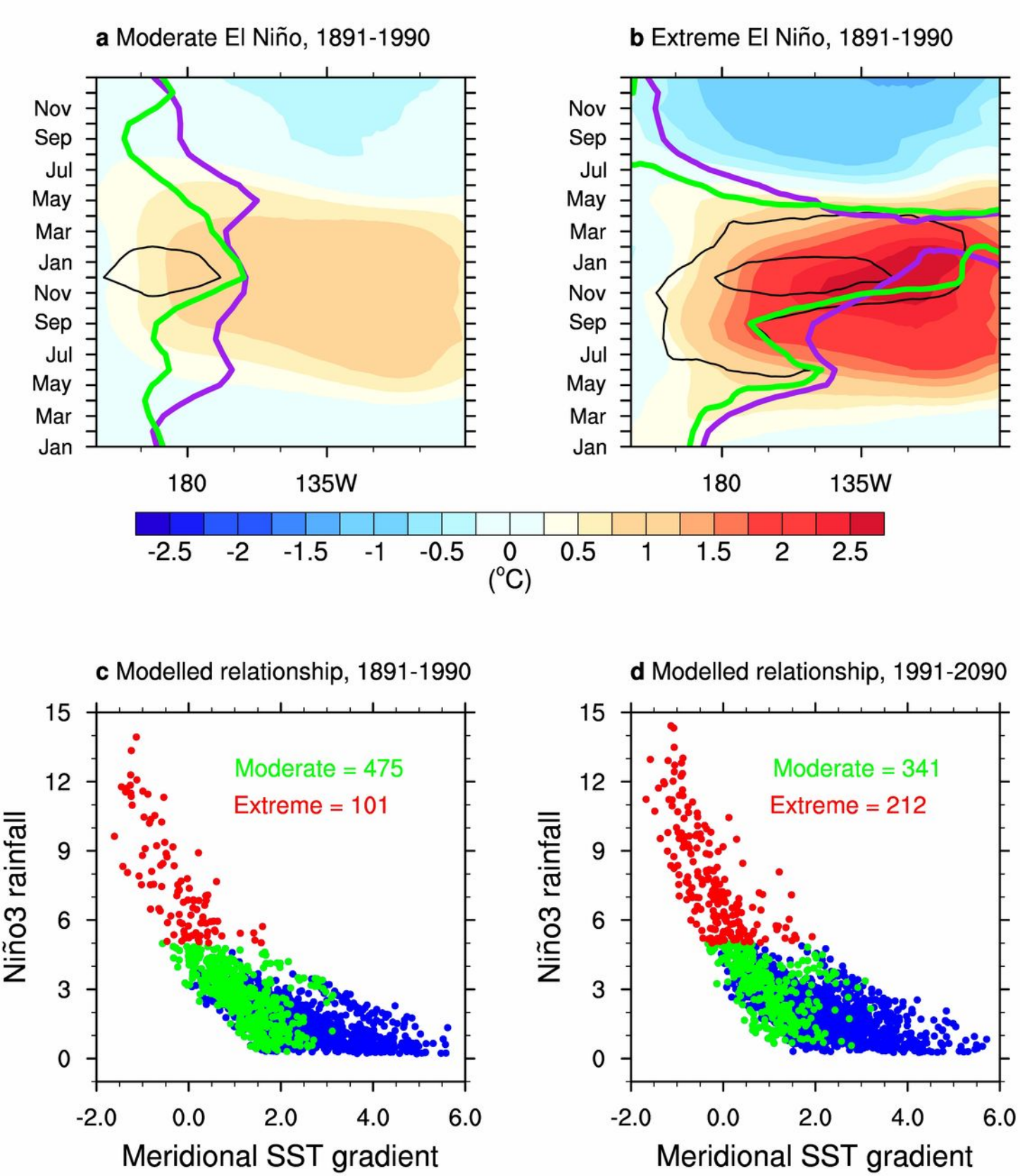
a Moderate El Niño, 1891-1990
b Extreme El Niño, 1891-1990
Nov
Sep
Jul
May
Mar
Jan
180
135W
-2.5
-2
-1.5
-1
-0.5
0
0.5
1
1.5
2
2.5
(°C)
c Modelled relationship, 1891-1990
d Modelled relationship, 1991-2090
Moderate = 475
Extreme = 101
Moderate = 341
Extreme = 212
Niño3 rainfall
Meridional SST gradient
15
12
9
6
3
0
-2.0
0.0
2.0
4.0
6.0

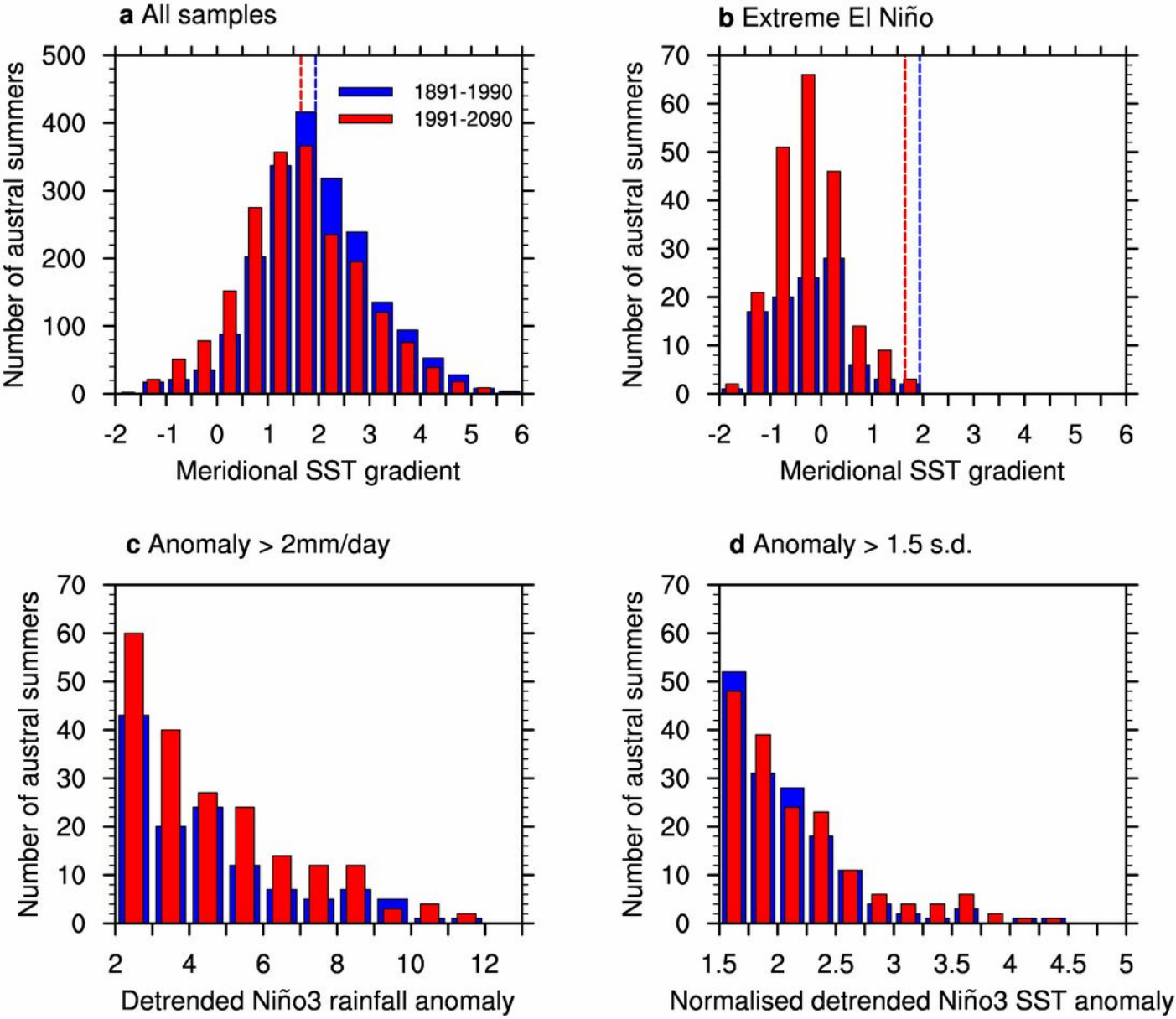
a All samples
1891-1990
1991-2090
Number of austral summers
Meridional SST gradient
b Extreme El Niño
Number of austral summers
Meridional SST gradient
c Anomaly > 2mm/day
Number of austral summers
Detrended Niño3 rainfall anomaly
d Anomaly > 1.5 s.d.
Number of austral summers
Normalised detrended Niño3 SST anomaly